Deuterium to hydrogen towards QSO 1009+2956 from a mesoturbulent model¹

Sergei A. Levshakov, David Tytler National Astronomical Observatory, Mitaka, Tokyo 181, Japan

and

Scott Burles
University of Chicago, 5640 S. Ellis Ave., Chicago, IL 60637

ABSTRACT

We present a new analysis of the deuterium absorption at z=2.504 towards the quasar Q1009+2956 using the mesoturbulent model which accounts for possible correlations in the large scale velocity field. We obtain a slightly higher deuterium-to-hydrogen ratio D/H $\simeq (3.5-5.0) \times 10^{-5}$ as compared with the recent measurement D/H = $(3.3-4.5) \times 10^{-5}$ (68% C.L.) performed by Burles & Tytler (1998b) using the usual microturbulent approximation which assumes that the velocity field is uncorrelated. Other mesoturbulent calculations of the D-abundances at z=3.572 towards Q1937–1009 and at z=0.701 towards Q1718+4807 (the systems showing 'low' and possibly 'high' D/H values, respectively, in the microturbulent approaches) agree with the present one within the errors of measurements. Thus, the mesoturbulent analysis does not reveal any spatial variations of D/H and supports the standard homogeneous model of big bang nucleosynthesis.

Subject headings: cosmology: observations — methods: data analysis — quasars: absorption lines — quasars: individual (1009+2956)

1. Introduction

High resolution spectra of the H+D absorption in Lyman limit systems towards distant quasars and the subsequent Voigt profile fitting analysis [VPF] suggested a dispersion in the primordial hydrogen isotopic ratio $D/H \equiv N(D~I)/N(H~I)$ (the ratio of the D I and H I column densities) of about one order of magnitude (see a short summary in Burles & Tytler 1998b).

¹Based on observations obtained at the W. M. Keck Observatory, which is jointly operated by the University of California and the California Institute of Technology.

This finding provoked a lively discussion in the literature on inhomogeneous models of big bang nucleosynthesis (e.g., Jedamzik & Fuller 1995; Webb et al. 1997; Kurki-Suonio et al. 1997). The standard (homogeneous) BBN predicts the same D/H abundance ratios in different directions in the early Universe since 'no realistic astrophysical process other than the Big Bang could produce significant D' (Schramm 1998, p.6). Deuterium is created exclusively in BBN and therefore we can expect that the D/H ratio decreases with cosmic time due to conversion of D into ³He and heavier elements in stars. It is clear that the precise measurements of the D/H values at high redshift are extremely important to probe whether BBN was homogeneous. The choice of the appropriate BBN model may in turn place constrains on different models of structure formation.

The lack of information about the nature of the absorption line broadening mechanism means that we might obtain different values of D/H if we make different assumptions. The multicomponent microturbulent models which are normally used assume that there is no correlation in the large scale velocity field. In these models both thermal and non-thermal velocities along the sight-line are represented by plain Gaussian distributions and the total velocity dispersion which is measured in high resolution spectra (b_{obs}) is given by $b_{obs}^2 = b_{therm}^2 + b_{turb}^2$. However, if there are correlations in the velocity field, the velocity distribution along a given line of sight may deviated significantly from the Gaussian model, i.e. $b_{obs}^2 \neq b_{therm}^2 + b_{turb}^2$. The application of the standard VPF analysis to such systems may then give incorrect D/H. We do not know, however, how to distinguish between the multicomponent microturbulent and one component mesoturbulent models if both of them show good fits to the spectral data.

To decide which model is better additional observations can be considered. For instance, if we assume that the Lyman limit systems arise in the outer regions of intervening galactic halos, then direct observations of the large scale flows in the giant Ly α emission halos at z > 2 (van Ojik et al. 1997), or in the star forming galaxies at $z \simeq 3$ (Pettini et al. 1998), or the complex metal absorption-line features in the quasar absorber/galaxy pairs at $z \sim 1$ (Bergeron et al. 1992; Bechtold & Ellinfson 1992; Charlton & Churchill 1998) may favor the mesoturbulent approximation since the rms turbulent velocity ($\sigma_t \equiv b_{turb}/\sqrt{2}$) in these halos ($\sigma_t \sim 20-100 \text{ km s}^{-1}$) is larger that the thermal width ($v_{th} \equiv b_{therm}$) of the hydrogen lines ($v_{th} \sim 13-15 \text{ km s}^{-1}$). The correlation effects become important if $\sigma_t/v_{th} \gtrsim 1$. Examples are given in Levshakov et al. (1997).

The first D/H measurement at z=2.504 towards Q1009+2956 was performed by Tytler & Burles (1997). They found D/H in the range from 2.2×10^{-5} to 4.2×10^{-5} . Later Burles & Tytler (1998b, hereafter BT) reconsidered this measurement including full coverage of the Lyman series and better quality data above and below the Lyman continuum break. Besides BT used the new method to measure D/H in quasar absorption systems described in Burles & Tytler (1998a). Considering six different microturbulent models, BT found D/H = $(3.9\pm0.6)\times10^{-5}$ which is consistent with their results on the z=3.572 system towards Q1937–1009 where D/H = $(3.3\pm0.3)\times10^{-5}$ (Burles & Tytler 1998a). Neither measurement is consistent with the D/H at z=0.701 towards Q1718+4807 deduced using the microturbulent model with a single component: D/H = $(2.0\pm0.5)\times10^{-4}$ (Webb et al. 1997), and D/H = 8×10^{-5} < D/H < 57×10^{-5} (Tytler

et al. 1998). This discord can be resolved using a more complex velocity model for Q1718+4807. Tytler et al. (1998) considered a second velocity component with the microturbulent model, while Levshakov et al. (1998) used a single component mesoturbulent model.

Here we apply the mesoturbulent model to Q1009+2956, and we conclude that all three QSOs may be described by a single value of D/H which is approximately equal to 4×10^{-5} .

2. The measurement of D/H

The present study is primarily aimed at the inverse problem in the analysis of the H+D Ly α absorption. The higher order Lyman series lines observed by BT (Ly β , Ly-6, Ly-12, Ly-13, Ly-14, Ly-20, and Ly-21) were also chosen in this analysis to restrict the set of possible velocity field configurations. We consider an absorbing region of thickness L which is a continuous medium (presumably the outer region of a foreground galaxy). The absorber is assumed to exhibit a mixture of bulk motions such as infall and outflows, tidal flows etc. Then the motion along the sight-line may be characterized by a fluctuating velocity field that we consider as a continuous random function of the space coordinate, v(s).

For simplicity, we assume a homogeneous density n_e and temperature T_{kin} . We have only weak justifications for these assumptions, which are necessitated by the complexity of the analysis. The assumption of constant T_{kin} may be supported by the fact that the states of thermally stable, optically thin interstellar gas take only restricted temperature ranges over a relatively wide range of density variations (see, e.g., Donahue & Shull 1991). The constant n_e seems to be quite plausible approximation for this particular z = 2.504 system since observational data show that metal lines from different ions show similar profiles. In Section 3 we use the similarity of C IV and Si IV profiles to estimate T_{kin} independently on the analysis of hydrogen lines. But these arguments do not rule out possible variations in T_{kin} and/or n_e in general. Our present mesoturbulent model is similar to that adopted in Levshakov $et\ al.\ (1998a,b)$.

We have developed a computational procedure which allows us to estimate physical parameters and simultaneously an appropriate velocity field structure along the sight-line. The details of the computational scheme based on the reverse Monte Carlo technique [RMC] are given in Levshakov et al. (1999). The algorithm requires to define a simulation box for the parameter vector $\theta = \{D/H, N(H I), T_{kin}, \sigma_t/v_{th}, L/l\}$; here l is the velocity field correlation length. The continuous random function v(s) is represented by its sampled values at equal space intervals Δs , i.e. by the sequence v_j (j = 1, 2, ..., k) of the velocity components parallel to the line of sight at the spatial points s_j . We describe v_j by a two-point Markovian process.

In the present study we adopt for the physical parameters the following boundaries: N(H I) ranges from 2.0×10^{17} to 3.0×10^{17} cm⁻², – the total hydrogen column density measured from the Lyman continuum optical depth by BT was found to lie in the interval $(2.1-2.8) \times 10^{17}$ cm⁻²; D/H – from 3.0×10^{-5} to 3.0×10^{-4} ; $T_{\rm kin}$ – from 10^4 to 2.5×10^4 K. For $\sigma_{\rm t}/v_{\rm th}$ the boundaries

were set from 1.0 to 2.5 to be typical for that observed in galactic halos. Since for $L/l \gg 1$ the meso- and microturbulent profiles tend to be identical (Levshakov & Kegel 1997), we consider here only moderate L/l ratios in the range 1 – 5. We do not assume that the D and H lines have identical velocities to the metal lines. The H I distribution is fixed by the higher order Lyman series lines. We fix z=2.503571 (the value adopted by BT) as the reference radial velocity at which v=0.

We use a χ^2 minimization routine and the RMC optimization technique to estimate five model parameters and the appropriate configuration of the velocity field v(s). Note that k components of the velocity field here are the 'nuisance parameters' and their number does not influence the physical parameters we are interested in. A lower bound to k is given by the inequality [cf. eq.(22) in Levshakov $et\ al.\ 1997$]:

$$\frac{L}{\Delta s} > \frac{L}{l} \frac{2}{\ln \left[1 - (v_{\rm th}/\sigma_{\rm t})^2\right]^{-1}},$$
(1)

with $\sigma_{\rm t}/v_{\rm th} > 1$.

In the Q1009+2956 spectrum, there are many absorption features blending the Lyman series lines. We do not fit these additional absorptions since they do not affect significantly the D/H measurement in this system, as shown by BT. The strongest absorption feature seen at z=2.50456 in Fig. 1 has, according to BT, N(H I) = 3.7×10^{13} cm⁻², which is less than 0.02% of the total N(H I) at z=2.504.

The portions of the Lyman series lines that, after preliminary analysis, were chosen as most appropriate to the simultaneous RMC fitting are indicated in Fig. 1 by the thick gray lines. In the standard χ^2 minimization, the following objective function is usually used

$$\mathcal{L} \equiv \chi^2 = \frac{1}{\nu} \sum_{i=1}^n \sum_{i=1}^{m_j} \frac{[I_i - F(\lambda_i, \theta)]^2}{\sigma_{I_i}^2} . \tag{2}$$

Here, I_i and σ_{I_i} are the observed normalized intensity and the experimental error within the *i*th pixel of the line profile, respectively. $F(\lambda_i, \theta)$ is the simulated intensity at the same *i*th pixel having wavelength λ_i . The total number of hydrogen lines is labeled by n, and the total number of data points $m = \sum_{j=1}^{n} m_j$, where m_j is the number of data points for the *j*th line. The number of fitted parameters p = 5, and $\nu = m - p$ is the degree of freedom ($\nu = 208$ in our case).

Equation (2) assumes that all λ_i -values are known exactly, and thus it ignores errors in the wavelength calibrations (λ -errors). These errors can be neglected in case of not very steep profiles and not very high SNR data, when small errors in λ leave the intensity within its uncertainty range, i.e.

$$I + \left| \frac{dI}{d\lambda} \right| \sigma_{\lambda} < I + \sigma_{I} ,$$

$$\left| \frac{dI}{d\lambda} \right| < \frac{\sigma_{I}}{\sigma_{\lambda}} , \tag{3}$$

or

where $\sigma_{\lambda} = \left(\sigma_{stat}^2 + \sigma_{system}^2\right)^{1/2}$ is the error of the wavelength scale calibration, and σ_I is the experimental uncertainty in I.

If, however, inequality (3) is violated, then the calibration errors, appearing in the shift of the line profile, lead to inappropriate high values of \mathcal{L} . To correct such solutions, we should adjust the λ scale. We have calculated (3) for different lines under consideration (see Table 1). From this table it is seen that (3) is strongly violated for the Ly α , Ly β and Ly-6 lines, but is fulfilled for the Ly-12 and higher order hydrogen lines.

To account for the λ -adjustment we incorporate new fitting parameters $\delta\lambda$ in equation (2) which now gets the form

$$\chi^2 = \frac{1}{\nu'} \left\{ \sum_{j=1}^n \sum_{i=1}^{m_j} \frac{\left[I_i - F(\lambda_i + \delta \lambda_j, \theta) \right]^2}{\sigma_{I_i}^2} + \sum_{j=1}^{n'} \left(\frac{\delta \lambda_j}{\sigma_{\lambda_j}} \right)^2 \right\} , \tag{4}$$

where the correction factor $\delta \lambda_j$ is common for all pixels of the jth hydrogen line. n' is the number of lines whose wavelength scales are to be corrected $(0 \le n' \le n)$, and $\sigma_{\lambda_j} \equiv \sigma_{\lambda} \simeq \frac{1}{4}$ FWHM. The number of fitted parameters in this case is p' = 5 + n' and hence $\nu' = m - p'$. In this approach possible values of $\delta \lambda_j$ are restricted and lie in the range $|\delta \lambda_j| < \sigma_{\lambda}$.

Using the original continuum as determined by BT (without allowing for errors in the local continuum in the vicinity of each hydrogen line) we found a few RMC profile fits which are listed in Table 2. We tried to find solutions with the reduced χ^2 per degree of freedom of $\chi^2_{min} \lesssim 1$. For all models from Table 2 the calculated hydrogen profiles are similar to that shown in Fig. 1. We do not find any large differences between calculated and real spectra. The under-absorption on the blue-ward side of D Ly α is probably caused by the Ly α forest lines. We do not treat this part of the spectrum because, in this case, unsaturated higher order Lyman series lines provide accurate predictions for the velocity of the deuterium Ly α line and its shape. Besides, as shown by BT, these additional absorptions do not affect significantly the D/H ratio in the z=2.504 system.

The derived v(s) configurations are not unique. But their projections – the radial-velocity distribution functions p(v) – are very much alike (see examples in Fig. 2). Figure 2 shows the p(v) distributions found by the RMC procedure (histograms) and for comparison p(v) for the best three-component microturbulent model 2 found by BT (thin-line Gaussians and their weighted sum shown by dotted-line). Both the RMC p(v) and the combined BT p(v) distributions show similar asymmetry. But the interpretation of these p(v) is different. In the microturbulent model the asymmetry is caused by the individual clouds with different physical parameters, whereas the mesoturbulent solution describes the homogeneously distributed gas with constant density and temperature along the sight-line.

Now comes the question about the most probable kinetic temperature and the accuracy of the approximation n_e = constant. Table 2 shows the spread of the T_{kin} values between 13700 K and 18100 K for different models. Each of these models is acceptable from the statistical point of view. To select the adequate models additional observational data should be taken into account. For

this purpose we consider below high SNR data on the unsaturated C IV and Si IV lines observed at the same z = 2.504 towards Q1009+2956.

3. The measurement of T_{kin} from metal absorption lines

We turn now to a brief discussion of the application of the Entropy-Regularized χ^2 -Minimization [ERM] procedure developed by Levshakov *et al.* (1998c, hereinafter LTA) to recover independently the kinetic temperature from the C IV and Si IV data obtained by BT. We suppose that H I and metals from the same Lyman limit system should give similar T_{kin} .

The ERM procedure utilizes complex but similar absorption line profiles of different ions to estimate a single value of T_{kin} for the whole absorbing region. The similarity of the complex profiles of ions with different masses and ionization potentials stems from the homogeneous gas density distribution along the sight-line, otherwise we would expect to observe different intensity fluctuations within the line profiles caused by variations of the local ionization parameter U which is the ratio of the density of ionizing photons to the total gas density. We consider the complex structure of the absorption lines as being generated by the large scale motions with the correlated internal structure. Satisfactory ERM solutions ($\chi^2_{min} \lesssim 1$) for a pair of lines of different ions will only exist when the homogeneous density approximation is consistent with the spectra.

The absorber in question is the outer part of the halo of a distant galaxy. The gas in the halo photo-ionized by QSOs is optically thin in the Lyman continuum. For such system the equilibrium temperature is weakly dependent on U (Donahue & Shull 1991). We may expect, therefore, that a single T_{kin} is still a suitable approximation in this case.

To estimate T_{kin} for the particular z=2.504 system, we have chosen C IV λ 1548 (SNR = 72) and Si IV λ 1394 (SNR = 73) lines observed with 8 km s⁻¹ spectral resolution (FWHM) by BT. We did not use the red components of these doublets because their data are more noisy. Applying the ERM procedure to the C IV λ 1548 and Si IV λ 1394 lines, we obtained the gas temperature $T_{kin}^* \simeq 13500$ K.

Figures 3 and 4 illustrate our results. The best-fitting profiles with three equidispersion components [for definition see eq.(12) in LTA] are shown in panels a and b of Fig. 3 by solid lines with the tick marks indicating the positions for the separate components. The choice of the appropriate $T_{kin}^* \simeq 13500$ K corresponding to the optimal value of the normalized regularization parameter $\hat{\alpha}_{opt} = 0.174$ is shown in Fig. 4. The objective function used in this case has the form

$$\mathcal{L}_{\alpha} = \chi^2 + \alpha \, \psi \,\,, \tag{5}$$

where ψ is a penalty function [eq.(21) in LTA] and the regularization parameter α is given by

$$\alpha = \alpha_{min} + \hat{\alpha} \left(\alpha_{max} - \alpha_{min} \right). \tag{6}$$

For this particular case $\alpha_{min} = -0.19$ and $\alpha_{max} = 0.05$ were chosen.

The obtained ERM estimation of $T_{kin}^* \simeq 13500$ K lies in the range of T_{kin} found by the RMC method from the H+D Ly α and higher order Lyman series profiles. Since the accuracy of the ERM solutions is shown to be about 10% (LTA), models **a**, **e**, and **g** in Table 2 seem to be consistent with the ERM result.

4. Conclusion

We have shown that the mesoturbulent model can explain the data adequately. In the following we discuss the relationship between the micro- and mesoturbulence models, and related issues.

The mesoturbulent model assumes constant T_{kin} and n_e but allows velocity correlations, while the microturbulent model allows different but constant T_{kin} and n_e for each of a finite number of components and assumes no coherent structure in the velocity field.

In the microturbulent approach it is explicitly assumed that the radial velocities are normally distributed so that the line profile is every time uniquely determined. In contrast, in the mesoturbulent approach we do not make the assumption of a Gaussian distribution for the radial velocities. This leads in turn to the concepts of randomness and unpredictability in the line formation process. That is to say, the apparent b-parameters usually measured in high resolution spectra may not be suitable to determine the true ratio σ_t/v_{th} which is used to estimate the relative importance of the non-thermal broadening (see Levshakov & Kegel 1997, for details).

In the two approaches, the D/H ratios are found to be similar for the particular z=2.504 system. However, microturbulent models yield slightly lower deuterium abundance and rather narrow range ($\simeq 15\%$) of its uncertainty. In the mesoturbulent solutions, although the total hydrogen column densities lie inside the range found by BT, the D/H values are less restricted because, in general, the radial-velocity distribution function p(v) is not known a priori. Our analysis gives a certain range for N(H I)_{tot} and D/H due to the finite signal-to-noise ratio and different p(v) configurations. This is shown in Fig. 5 where different confidence regions for this pair of physical parameters are depicted for models $\bf a$, $\bf e$, and $\bf g$ under the assumption that the other parameters $T_{\rm kin}$, $\sigma_{\rm t}/v_{\rm th}$, L/l and v(s) are fixed (the computing procedure is described in Levshakov et al. 1999). The estimated D-abundance towards Q1009+2956 [D/H $\simeq (3.5-5.0)\times 10^{-5}$] agrees within the errors of measurement with the RMC results for the D I absorption systems seen towards Q1937-1009 [D/H $\simeq (3.8-4.8)\times 10^{-5}$: Levshakov et al. 1998a] and towards Q1718+4807 [D/H $\simeq (3.0-7.5)\times 10^{-5}$: Levshakov et al. 1998b, Levshakov 1998].

In general, accurate measurement of D/H requires (i) correct modeling, (ii) treatment of continuum placement errors reported by Burles & Tytler (1998a,b), and (iii) treatment of contaminating absorption.

We conclude that the current observations support SBBN and that there is no conflict

with the D/H measurements in these three Lyman limit systems. A single and robust value of D/H $\simeq 4 \times 10^{-5}$ is sufficient to describe H+D profiles within the framework of the mesoturbulent model.

S.A.L. and D.T. gratefully acknowledge the hospitality of the National Astronomical Observatory of Japan where this work was performed.

REFERENCES

- Bechtold, J., & Ellingson, E. 1992, ApJ, 396, 20
- Bergeron, J., Cristiani, S., & Shaver, P. 1992, A&A, 257, 417
- Burles, S., & Tytler, D. 1998a, ApJ, 499, 699
- Burles, S., & Tytler, D. 1998b, ApJ, 509, in press [BT]
- Charlton, J., & Churchill, C. W. 1998, ApJ, 499, 181
- Fixsen, D. J., Cheng, E. S., Gales, J. M., Mather, J. C., Shafer, R. A., & Wright, E. L. 1996, ApJ, 473, 576
- Donahue, M., & Shull, J. M. 1991, ApJ, 383, 511
- Jedamzik, K., & Fuller, G. M. 1995, ApJ, 452, 33
- Kurki-Suonio, H., Jedamzik, K., & Mathews, G. J. 1997, ApJ, 479, 31
- Levshakov, S. A. 1998, in the Proceedings of the Xth Rencontres de Blois 'The Birth of Galaxies' (June 22 July 4, 1998, Blois, France), in press (astro-ph/9808295)
- Levshakov, S. A., & Kegel, W. H. 1997, MNRAS, 288, 787
- Levshakov, S. A., Kegel, W. H., & Mazets, I. E. 1997, MNRAS, 288, 802
- Levshakov, S. A., Kegel, W. H., & Takahara, F. 1998a, ApJ, 499, L1
- Levshakov, S. A., Kegel, W. H., & Takahara, F. 1998b, A&A, 336, L29
- Levshakov, S. A., Kegel, W. H., & Takahara, F. 1999, MNRAS, 302, 707
- Levshakov, Takahara, F., & Agafonova, I. I. 1998c, ApJ, submit. (astro-ph/9809166) [LTA]
- Pettini, M., Kellogg, M., Steidel, C. C., Dickinson, M., Adelberger, K. L., & Giavalisco M. 1998, ApJ, in press (astro-ph/9806219)
- Schramm, D. N. 1998, in Primordial Nuclei and Their Galactic Evolution, eds. N. Prantzos, M. Tosi, & R. von Steiger (Kluwer Academic Publ.: Dordrecht, The Netherlands), 3
- Tytler, D., & Burles, S. 1997, in Origin of Matter and Evolution of Galaxies, eds. T. Kajino, Y. Yoshii, & S. Kubono (World Scientific Publ. Co.: Singapore), 37
- Tytler, D., Burles, S., Lu, L., Fan, X.-M., Wolfe, A., & Savage, B. D. 1998, AJ, in press (astro-ph/9810217)
- van Ojik, R., Röttgering, H. J. A., Miley, G. K., & Hunstead, R. W. 1997, A&A, 317, 358

Webb, J. K., Carswell, R. F., Lanzetta, K. M., Ferlet, R., Lemoine, M., Vidal-Madjar, A., & Bowen, D. V. 1997, Nature, 388, 250

This preprint was prepared with the AAS IATEX macros v4.0.

- Fig. 1.— Observations (normalized flux) and RMC fits for Q1009+2956. The Keck/HIRES echelle data obtained by BT dots and 1σ error bars; the calculated RMC profiles (model **a** in Table 2) convolved with the instrumental resolution of FWHM = 8 km s⁻¹ solid curves. The thicker grey parts of these curves show the regions about each Lyman line used in the fitting procedure. The redshift of this Lyman limit system is z = 2.503571, according to BT.
- Fig. 2.— Radial-velocity distribution functions p(v) of the RMC solutions for models \mathbf{a} , \mathbf{e} , and \mathbf{g} (solid, dashed and dotted line histograms, respectively) and for comparison three p(v) distributions with the velocity dispersions $b(\mathbf{H}) = 16.0$, 16.8, and 24.6 km s⁻¹ (solid curves) adopted from the best fit microturbulent model 2 of BT. The curves are weighted by the corresponding hydrogen column densities of 1.29×10^{17} , 0.50×10^{17} and 0.24×10^{17} cm⁻². The sum of all three weighted functions is shown by the dotted curve.
- Fig. 3.— (a,b) Normalized data points with 1σ error bars for HIRES echelle spectrograph observations (FWHM = 8 km s⁻¹) on the Keck telescope of the C IV λ 1548 (SNR = 72) and Si IV λ 1394 (SNR = 73) at the redshift z=2.503571 towards the quasar Q1009+2956 (BT). The ERM result (reduced $\chi^2=0.92$ with 37 degrees of freedom) for C IV and Si IV (solid lines) is based on simultaneously fitting the multiple equidispersion lines located at the positions shown by the tick marks at the top of each panel. The evaluated kinetic temperature $T^* \simeq 13500$ K is plotted in panel a.
- Fig. 4.— An example of the Entropy-Regularized χ^2 -Minimization [ERM] technique used to measure the kinetic temperature from the complex absorption spectra of the C IV and Si IV lines shown in Fig. 3. The filled circles connected by dotted line show the normalized values of the cross-entropy $\hat{\mathcal{K}}$ as function of the normalized regularization parameter $\hat{\alpha}$. The dashed curve is the normalized curvature of the $\hat{\mathcal{K}}(\hat{\alpha})$ trajectory. Its maximum at point $\hat{\alpha}=0.174$ corresponds to the kinetic temperature $T^*\simeq 13500$ K which is indicated by arrows. For more details (especially on the ERM technique) the reader is encouraged to consult LTA.
- Fig. 5.— Confidence regions (68% confidence level) in the plane 'N(H I)–D/H' for solutions \mathbf{a} , \mathbf{e} , and \mathbf{g} listed in Table 2. Different solutions give different contours. The other parameters of models \mathbf{a} , \mathbf{e} , and $\mathbf{g} T_{\text{kin}}$, $\sigma_{\text{t}}/v_{\text{th}}$, and L/l and the corresponding configurations of the velocity fields v(s) are fixed. The size of the confidence region depends on signal to noise. The letters a, e, and g mark the points of maximum likelihood for models \mathbf{a} , \mathbf{e} , and \mathbf{g} (see Table 2).

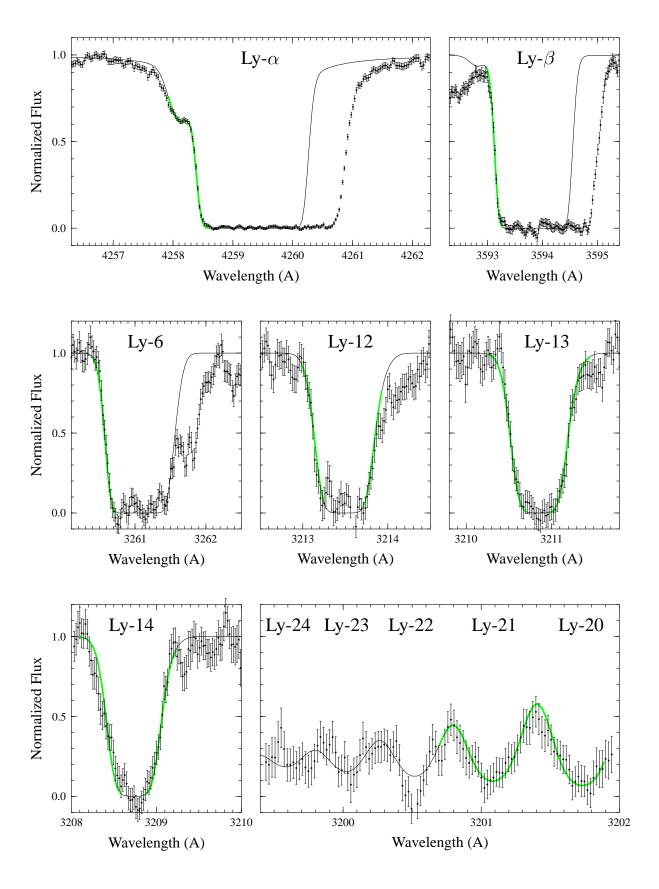
Table 1. H I data for the λ -adjustment criterion (eq.(3)).

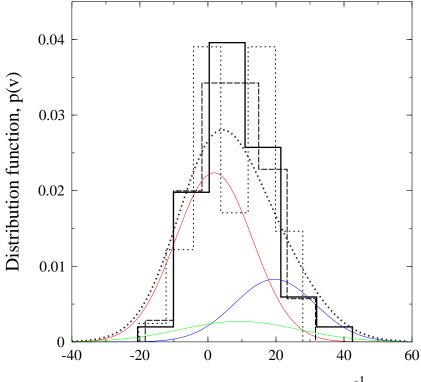
	$\mathrm{Ly}lpha$	$\mathrm{Ly}eta$	Ly-6	Ly-12
$\lambda\lambda$, Å	4258.30 -	3593.01 -	3260.50 -	3213.03 -
	4258.50	3593.21	3260.66	3213.21
$\langle SNR \rangle$	80	36	17	13
$\sigma_I/\sigma_\lambda, {\rm \AA}^{-1}$	0.4	1.0	3.0	4.0
$dI/d\lambda$, Å ⁻¹	3.0	4.0	5.0	4.0

Table 2. Model parameters derived from the Lyman series lines by the RMC method.

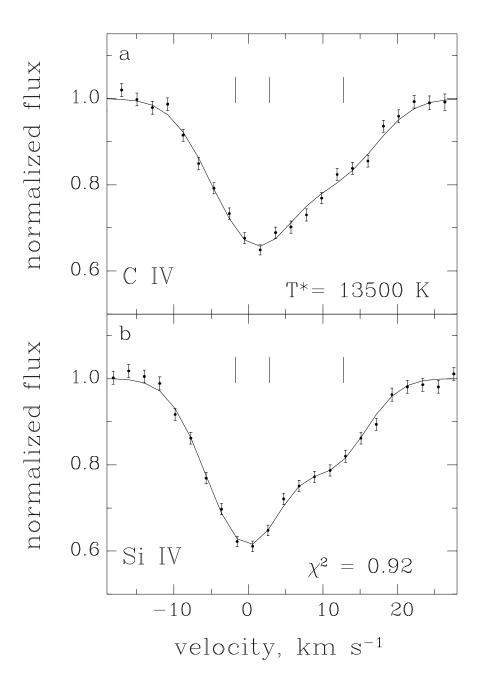
Model	D/H	N_{17}	T_4	$\sigma_{ m t}/v_{ m th}$	L/l	χ^2_{min}	$\delta \lambda_{lpha}$	$\delta \lambda_{eta}$	$\delta\lambda_6$
(\mathbf{a})	3.76	2.37	1.38	1.75	2.03	0.80	0.018	-0.019	-0.022
(\mathbf{b})	4.26	2.17	1.81	1.18	2.18	0.84	0.028	-0.014	-0.022
(\mathbf{c})	4.34	2.20	1.57	2.00	1.68	0.73	0.021	-0.013	-0.022
(\mathbf{d})	4.37	2.20	1.55	1.58	2.17	0.73	0.026	-0.011	-0.022
(e)	4.39	2.16	1.51	1.58	1.65	0.72	0.023	-0.014	-0.022
(\mathbf{f})	4.51	2.19	1.64	1.09	2.03	0.83	0.023	-0.015	-0.022
(\mathbf{g})	4.65	2.15	1.37	1.17	3.70	0.71	0.026	-0.011	-0.022

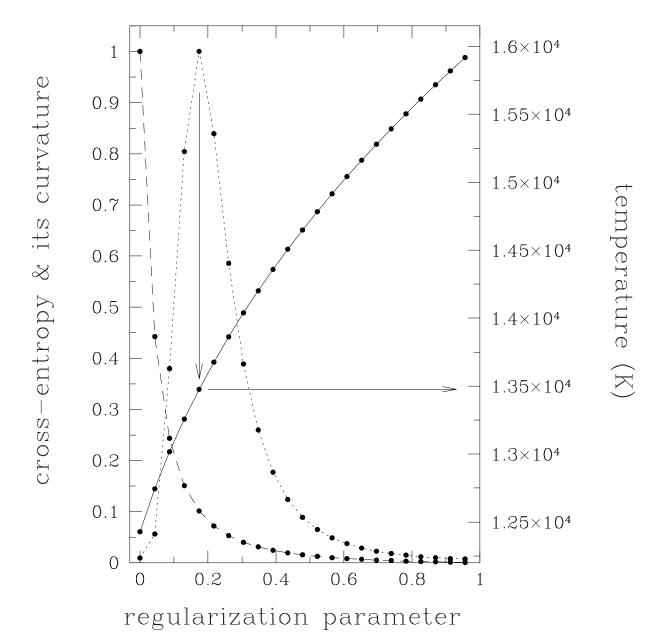
^a N₁₇ is the total hydrogen column density in units of 10^{17} cm⁻², D/H in units of 10^{-5} , T_4 kinetic temperature in units of 10^4 K, $\delta\lambda_j$ adjustment factor in Å, where $\delta\lambda_\alpha$, $\delta\lambda_\beta$, and $\delta\lambda_6$ are the wavelength corrections for Ly α , Ly β , and Ly-6, respectively.

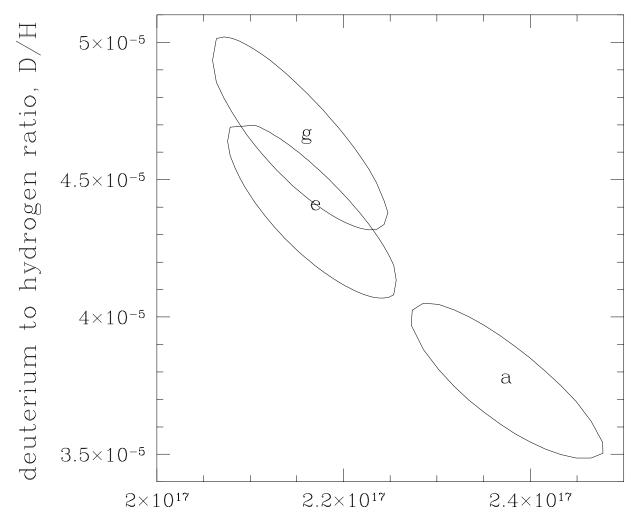




Relative radial velocity, v (km s⁻¹)







hydrogen column density (cm⁻²)